ACS Photonics

Letter

pubs.acs.org/journal/apchd5

Super-Resolution Structured Pump−Probe Microscopy

Eric S. Massaro,[†] Andrew H. Hill,[‡] and Erik M. Grumstrup*[,†,‡]

[†]Department of Chemistry and Biochemistry and [‡]Montana Materials Science Program, Montana State University, Bozeman, Montana 59717, United States

Supporting Information

ABSTRACT: Imaging excited-state dynamics in complex materials provides an important avenue for understanding the role played by micro- and nanoscale structural and compositional heterogeneity in the performance of active electronic and optoelectronic devices. Here, we develop structured pump−probe microscopy (SPPM), a subdiffraction-limited, time-resolved microscopy that incorporates a focused diffraction-limited probe field together with a spatially modulated pump excitation field. We apply the technique to study free carrier dynamics in silicon nanowires, demonstrating far-field ultrafast time-resolved spectroscopy with a 114 nm point-spread function while remaining in the perturbative excitation regime. We predict SPPM will provide an accessible approach for characterizing the ultrafast dynamics of subwavelength regions in complex materials systems.

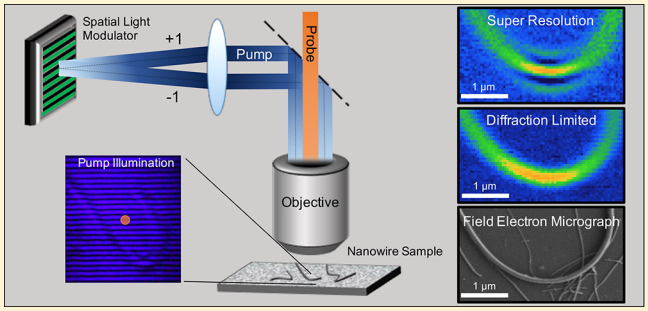

KEYWORDS: *super-resolution, structured illumination microscopy, transient absorption microscopy, nonlinear microscopy*

Pump−probe microscopy is a powerful tool for studying nonequilibrium dynamics in a variety of complex materials systems including nanostructures, low-dimensional semiconductors, and material interfaces. The simultaneous submicrometer spatial resolution and femtosecond temporal resolution enabled by the technique provides detailed, structurally correlated insights into intraparticle heterogeneity,[1−3] free carrier transport,[4−6] surface plasmon propagation,[7] and unique interfacial states,[8−11] which are inaccessible with conventional spectroscopies or microscopies. However, like all diffraction-limited optical techniques, the spatial resolution of pump−probe microscopy is restricted to probe areas greater than ∼200 nm.

Imaging at length scales smaller than 200 nm requires approaches that circumvent the limits of lens-based diffractive microscopes. While a number of fluorescence-based microscopies,[12−18] electron microscopies (SEM and TEM[19]), and atomic force microscopy (AFM[20]) substantially improve spatial resolution, these techniques provide little or no dynamical information. To interrogate transient dynamics on subdiffraction-limited length scales, several approaches have been employed. Tip-enhanced techniques that couple ultrafast laser pulses together with a subwavelength scanning probe can resolve ultrafast dynamics on length scales far below the diffraction limit.[21,22] While highly promising, these measurements are complicated by a large far-field background that must be discriminated from the desired tip-localized signal and by perturbations introduced by system−probe tip coupling, which can affect the observed material dynamics. Far-field approaches are experimentally simpler and can provide insight into electronic environments isolated from the surface.[23] A pump−probe analog to stimulated emission depletion microscopy (STED) was recently reported, in which a third shaped laser pulse temporally spaced between the pump and probe pulses saturates an annular region surrounding the central excitation spot.[24] While this approach narrows the effective point-spread function of the microscope, the third intense saturation pulse can cause photobleaching and highly nonlinear light−matter interactions, which may be problematic for both imaging and spectroscopic applications. A similar approach utilizes differential transient absorption in place of saturable absorption, retaining the use of a third pump pulse in order to confine the dimensions of the pump−probe response in both linear and nonlinear regimes.[25]

Here we develop structured pump−probe microscopy (SPPM), which employs a modulated pump excitation field to provide ultrafast spectroscopic measurements of subdiffraction-limited sample areas. As a demonstration of our approach, we utilize SPPM to characterize free carrier dynamics in silicon nanowires (NWs) and show the technique can achieve an effective point-spread function (PSF) with ∼114 nm full width at half-maximum (fwhm). These results suggest conventional far-field optics, in conjunction with spatial pulse shaping, may provide an experimentally accessible approach for interrogating dynamics of complex materials systems with sub-100 nm spatial resolution.

Received: September 24, 2015
Published: March 2, 2016

DOI: 10.1021/acsphotonics.6b00140
ACS Photonics 2016, 3, 501−506

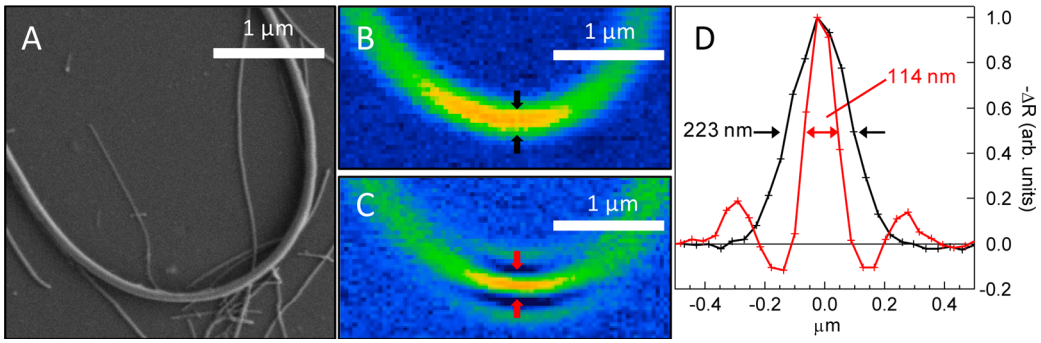

Figure 1. Comparison of diffraction-limited and structured pump–probe microscopy. (A) Field emission electron micrograph of a 100 nm diameter silicon nanowire. (B) Diffraction-limited pump–probe image of the NW in panel A at Δt = 0 ps. (C) SPPM image achieved through reconstruction. (D) Line width comparison at positions indicated by the arrows in the two pump–probe images. Black, diffraction limited; red, SPPM.

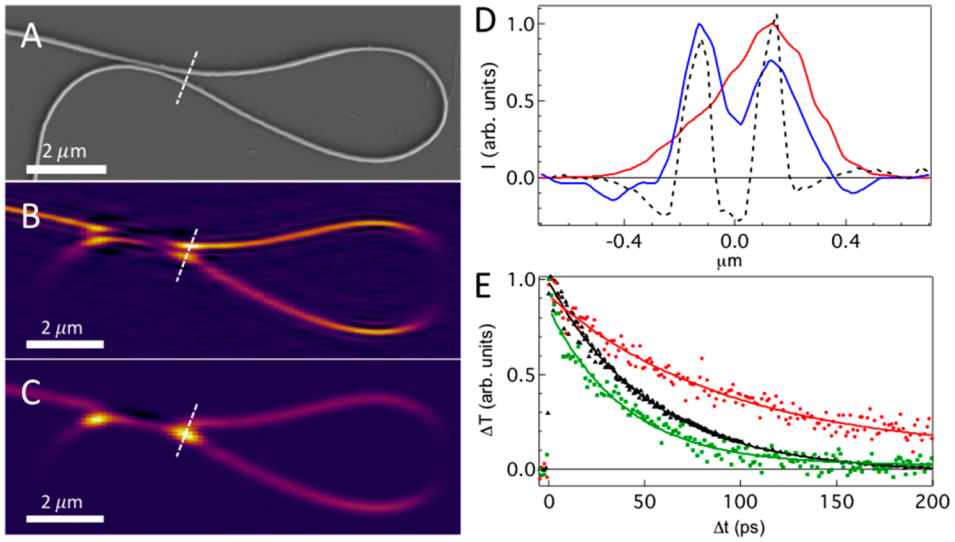

Figure 2. SPPM spatial resolution enhancement and subdiffraction limit spectroscopic characterization. (A) Field emission micrograph of a single 140 nm silicon nanowire. (B) SPPM image with enhanced resolution along the *y*-axis. (C) Diffraction-limited pump–probe image of the nanowire in panel A taken at Δt = 0 ps. (D) Line-shape comparisons of diffraction-limited pump–probe (red) and SPPM images (blue) of panels B and C taken from location indicated by a dashed line in each panel. Also shown is the profile taken from the SEM (black, dashed). (E) Transient kinetics collected from image region spanned by the dashed lines in panels B and C. Traces 1 (red) and 2 (green) were collected with enhanced spatial resolution and show the NW has different recombination kinetics along its length. Trace 3 (black) represents kinetics collected using standard diffraction-limited pump–probe microscopy. The diffraction-limited kinetics average over the dynamics of both NW regions.

STRUCTURED PUMP–PROBE IMAGING AND SPECTROSCOPY

To achieve the improved PSF of SPPM, we use a computer-programmable digital micromirror device (DMD) encoded with a fringe pattern to create a sinusoidally modulated pump field at the focus of the microscope objective (0.9 NA). A diffraction-limited probe pulse is spatially overlapped with the pump field, and the NW sample is raster scanned to produce a pump–probe image at a well-defined delay time, Δt. Because the induced polarization of the sample depends on the product of the pump intensity and the probe field, the effective pump–probe excitation field is spatially modulated. By combining images collected with three different pump pattern phases (details below), the spatial modulation in the images provides access to additional high (spatial)-frequency information that is inaccessible with conventional approaches.

Figure 1 presents the enhanced imaging capability provided by SPPM. Panel A shows a field emission micrograph of a 100 nm diameter silicon nanowire (NW1) deposited on a quartz substrate. A diffraction-limited pump–probe image of the same NW is shown in panel B. To collect the image, the λ = 400 nm pump and λ = 585 nm probe beams were spatially overlapped at the sample plane and the NW was raster scanned with a piezoelectric translation stage. The spatial resolution of the image in this modality is determined by the product of overlapping pump and probe spot sizes. Panel C shows the SPPM image of the same NW. In this image, the PSF is improved by nearly a factor of 2 relative to conventional pump–probe imaging. The improvement can be more clearly seen in a comparison of the diffraction-limited and SPPM profiles plotted in panel D; whereas the conventional approach produces a fwhm of 223 nm, the SPPM image has a line width of 114 nm. Note that due to the low diffraction efficiency of the DMD at 400 nm, our optical apparatus limits the improved PSF to the *y*-axis only. However, isotropic enhancement can be readily achieved by implementing a two-dimensional pump modulation scheme and performing a multidimensional image reconstruction.

Figure 2 presents a second comparison of diffraction-limited and SPPM approaches. Panels A, B, and C of Figure 2 show

DOI: 10.1021/acsphotonics.6b00140
ACS Photonics 2016, 3, 501–506

field emission microscopy (FEM), diffraction-limited, and SPPM images, respectively, of a single Si NW that is bent in a hairpin geometry. Comparison of the images in panels B and C shows that, in contrast to conventional pump−probe microscopy, SPPM is capable of resolving the two regions of the NW in close proximity. The increase in spatial resolution can be more clearly seen in panel D, where profiles of the two images taken from the locations indicated by the dashed lines are shown together with a profile taken from the FEM. Simulated line shapes shown in Supporting Information confirm this finding, revealing that diffraction-limited pump−probe microscopy does not resolve two NWs spaced 250 nm apart (Figure S1). In contrast, the simulated SPPM line shapes show a clear modulation of signal intensity between the two features, as we observe experimentally. We note that both diffraction-limited pump−probe and SPPM imaging show anomalous behavior when the NW is within ∼200 nm of itself (see region to the left of the dashed line in panels B and C). These effects, which manifest as a change in signal sign, likely arise from optical system aberrations and interference of the field radiating from two image regions; however a detailed understanding requires further investigation.

While the increased imaging resolution represents an improvement over the diffraction limit, it is the ability to acquire ultrafast spectroscopic information from a subdiffraction-limited volume that makes SPPM particularly valuable for characterizing complex materials systems. Panel E shows a comparison of the kinetics collected with the enhanced resolution and diffraction-limited approaches. Within the context of the imaging modality discussed above, an SPPM kinetics trace can be understood as a single-pixel image, collected at multiple delay times, Δt. Three individual kinetics traces are collected with shifted pump field patterns and combined to produce the SPPM kinetics trace that reports on the dynamics of a subdiffraction-limited sample volume. Photoexcitation of silicon nanowires at 400 nm is known to produce free charge carriers, which primarily decay through surface recombination.[26] The SPPM kinetics traces in Figure 2 are consistent with this mechanism and show the two regions of the NW have slightly different surface recombination velocities of 3.8×10^4 cm/s (1) and 8.8×10^4 cm/s (2).[27] In contrast, the diffraction-limited measurement shows a surface recombination velocity of 6.5×10^4 cm/s (3), a value that reflects a weighted average of the individual NW recombination velocities.

While a full theoretical treatment is beyond the scope of this Letter, we briefly describe the imaging theory for diffraction-limited pump−probe microscopy and SPPM below.

DIFFRACTION-LIMITED PUMP−PROBE MICROSCOPY

At the focus of a diffraction-limited pump−probe microscope, the homodyne-detected signal is proportional to the product of the probe field with the sample's nonlinear polarization.[28,29] As such, the diffraction-limited pump−probe image can be expressed as the convolution of the object function ($o(r)$) with the electric field components (E_1, E_2), each convolved with its respective coherent PSF, $h_1(r)$ (pump) or, $h_2(r)$ (probe):

$$\begin{aligned} I_{\mathrm{DL}}(r) &= o(r) \otimes |E_1(r) \otimes h_1|^2 |E_2(r) \otimes h_2|^2 \\ &= o(r) \otimes (\delta(r) \otimes h_1)^2 \cdot (\delta(r) \otimes h_2)^2 \\ &= o(r) \otimes {h_1}^2 \cdot {h_2}^2 \end{aligned} \tag{1}$$

The object function contains the spatial distribution of the imaged object, as well as its third-order nonlinear susceptibility. The Fourier transform of eq 1 yields the conjugate space description of the diffraction-limited image:

$$\tilde{I}_{\mathrm{DL}}(k) = \tilde{O}(k) \cdot (\tilde{H}_1 \otimes \tilde{H}_1 \otimes \tilde{H}_2 \otimes \tilde{H}_2) \tag{2}$$

We use capital letters to indicate the conjugate of a Fourier transform pair. Equation 2 describes the conjugate image, $\tilde{I}_{\mathrm{DL}}(k)$, as the product of the object spectrum, $\tilde{O}(k)$, and the convolution of the coherent optical transfer functions (OTFs), $\tilde{H}_n(k)$. The coherent OTFs for the pump and probe are determined by the imaging system and, in the absence of optical aberrations, act as perfect cutoff filters, whereby all frequency components within the passband are transmitted unaltered, and all others are completely attenuated. The convolution of OTFs in eq 2 defines an effective low-pass filter, which attenuates the high-frequency components (of $\tilde{O}(k)$) passing through the imaging system. Thus, the extent of high-frequency attenuation by the OTFs defines the ultimate spatial resolution of the imaging system: the more high-frequency information is transmitted, the better the spatial resolution of the image.

STRUCTURED PUMP−PROBE MICROSCOPY

To provide the enhanced resolution imaging and spectroscopy capabilities of SPPM, we use a sinusoidally modulated pump field rather than the diffraction-limited fields of eq 1. The ±1 diffraction orders produced from the DMD are selected with a spatial mask and directed toward the back aperture of the microscope objective. These mutually coherent beams are imaged onto the sample plane to produce a sinusoidally modulated fringe pattern, which arises from interference between the two orders propagating along the $+k_r$ and $-k_r$ directions. The probe beam is then spatially overlapped with the pump pattern, and the sample is raster scanned to produce an image. The structured pump−probe image collected under these excitation conditions is

$$\begin{aligned} I_{\mathrm{str}}(r;\varphi) &= o(r) \otimes |E_1(r) \otimes h_1|^2 |E_2(r) \otimes h_2|^2 \\ &= o(r) \otimes |\exp(ik_r r + \varphi) + \exp(-ik_r r - \varphi)|^2 \cdot \\ &\quad (\delta(r) \otimes h_2)^2 \\ &= o(r) \otimes [1 + \cos(2k_r + 2\varphi)] \cdot {h_2}^2 \end{aligned} \tag{3}$$

Here we have assumed that the frequency components (at $\pm k_r$) lie within the passband of the imaging system and are therefore transmitted to the sample plane unaltered. The Fourier transform of eq 3 is the conjugate space description of the structured pump−probe image:

$$\begin{aligned} \tilde{I}_{\mathrm{str}}(k;\varphi) = \tilde{O}(k) \cdot \Big(\Big[&\frac{1}{2}\delta(k - 2k_r)e^{i2\varphi} + \delta(k) \\ &+ \frac{1}{2}\delta(k + 2k_r)e^{-i2\varphi} \Big] \otimes \tilde{H}_2 \otimes \tilde{H}_2 \Big) \end{aligned} \tag{4}$$

which can be rewritten as

DOI: 10.1021/acsphotonics.6b00140
ACS Photonics 2016, 3, 501−506

$$\tilde{I}_{str}(k;\varphi) = \tilde{O}(k)\cdot\left(\frac{1}{2}\tilde{H}_2'(k-2k_r)e^{i2\varphi} + \tilde{H}_2'(k) + \frac{1}{2}\tilde{H}_2'(k+2k_r)e^{-i2\varphi}\right) \quad (5)$$

with $\tilde{H}_2' = \tilde{H}_2 \otimes \tilde{H}_2$.

The sinusoidal pump intensity and phase are controlled by encoding a pattern on the DMD positioned at an image plane of the microscope. Figure 3A shows one such pattern, which is composed of a periodic array of 6 "on" and 6 "off" pixels. The corresponding pump intensity as recorded by a camera placed at a second image plane of the microscope is shown in panel B. Panel C shows a phase-shifted DMD pattern with $\varphi = \pi/2$. In this case, the corresponding pump field intensity (panel D) is spatially shifted by π relative to that in panel B. The factor of 2 difference stems from the coherent interference of the two counter-propagating pump fields (note the factors of 2 in the cosine term in eq 3).

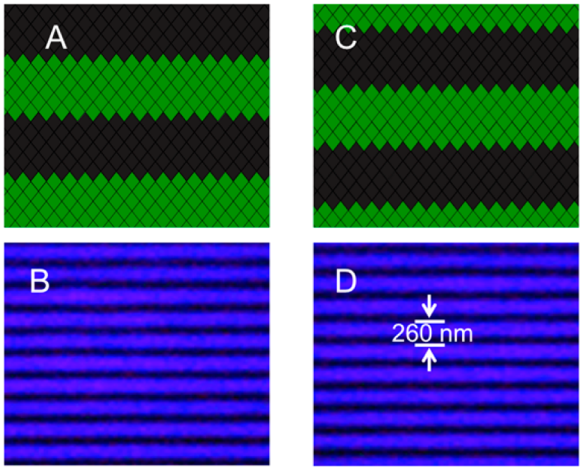

Figure 3. Phase variation of the DMD-generated modulated pump pattern. (A, C) Mirror positions (green, "on"; black, "off") encoded on the DMD to produce the pump intensity modulation. Panels A and C have a $\pi/2$ relative phase shift. (B) Camera image of the 0 phase offset modulation pattern. (D) Camera image of the $\pi/2$ phase shifted pattern. The camera images have a relative phase shift of π due to interference of the two first-order diffractions.

To generate enhanced resolution images like panel C of Figure 1, three images, $I_{str}(r;\varphi)$, are collected for three unique pump phases, $0 \le \varphi < \pi$. The phase shift of the pump pattern causes variation in the spatial profile of the pump−probe overlap region as the relative orientation of the focused probe beam and the modulated pump pattern changes. This effect is illustrated in Figure 4, where structured pump−probe images at $\Delta t = 0$ ps are shown for DMD phases of $\varphi = 0$ (panel A) and $\varphi = \frac{\pi}{2}$ (panel B). In panel A, the minimum of the pump intensity is roughly centered in the probe spot, whereas a maximum is centered for panel B. Panel C of Figure 4 shows profiles of the two images in the locations indicated by the dashed lines.

Reconstruction of the enhanced resolution image proceeds by solving the linear system of equations defined by the three images collected with different phases $\{\varphi_1, \varphi_2, \varphi_3\}$ and isolating the three components of eq 5 centered at $2k_r$, 0, $-2k_r$.[30−32] The processed enhanced-resolution image in conjugate space is then given by

$$\tilde{I}_{SPPM}(k) = \tilde{O}(k)\cdot(\tilde{H}_2'(k-2k_x) + \tilde{H}_2'(k) + \tilde{H}_2'(k+2k_x)) \quad (6)$$

Comparison between eq 6 and eq 2 shows that the diffraction-limited and SPPM images have a similar form, in which the conjugate space object function, $\tilde{O}(k)$, is filtered by an effective OTF. The functional form of the OTF differs between the two images; however provided the term in parentheses in eq 6 transmits more high frequency information, $I_{SPPM}(r)$ will have better spatial resolution. A comparison of diffraction-limited and SPPM conjugate space images is shown in Figure S2.

In summary, we have developed far-field, subdiffraction-limited pump−probe microscopy utilizing a spatially structured pump excitation field. The point-spread function of SPPM is smaller than the diffraction limit by nearly a factor of 2. The enhanced spatial resolution achieved by the technique provides a facile approach for interrogating transient dynamics of interfaces, nanostructures, and nanoscale domains in complex materials with substantially greater precision. While we report imaging line widths of 114 nm fwhm, a higher numerical aperture objective (NA 1.4) may enable further improved spatial resolution, substantially broadening the scope of far-field transient microscopy for characterizing complex materials and biological systems.

METHODS

A schematic of our home-built pump−probe microscope is presented in Figure 5. A portion of the output from a femtosecond Ti:sapphire oscillator (Spectra Physics MaiTai:

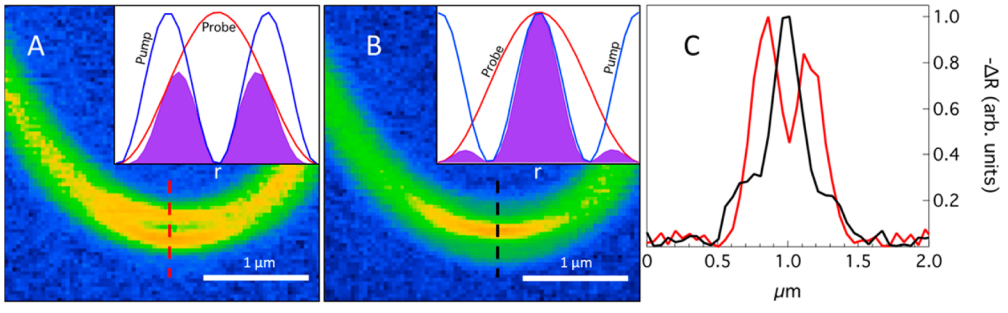

Figure 4. Pump−probe images of silicon nanowires with structure pump excitation. (A) Probe spot centered on a minimum of the modulated pump pattern. (B) Probe spot centered over the top of an individual pump peak. The insets in panels A and B illustrate the effective excitation field in their respective panels. Panel C shows the intensity profile of both images with slices taken at the red and black dashed lines in panels A and B, respectively.

DOI: 10.1021/acsphotonics.6b00140
ACS Photonics 2016, 3, 501−506

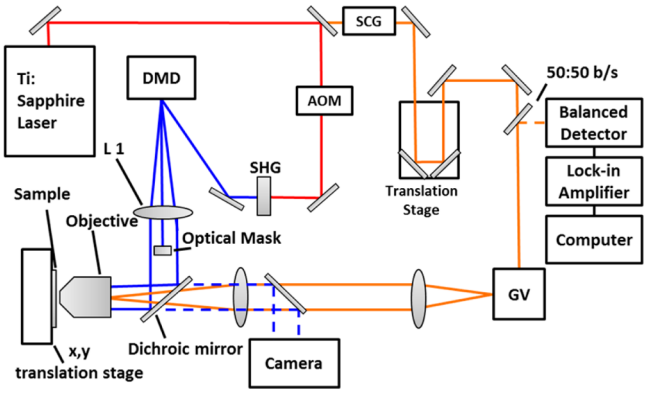

Figure 5. Schematic of DMD-based structured pump−probe microscope.

800 nm, 79 MHz, 90 fs fwhm) is split to produce pump and probe paths. The pump line is coupled into an acoustooptic modulator before frequency doubling in a β-barium borate crystal to produce 400 nm excitation pulses (23 pJ/pulse). The pump beam is directed toward the DMD (Texas Instruments DLP Lightcrafter) to produce ±1 diffraction orders, which are collected with a tube lens (L1). The DMD produces many diffraction orders, which must be optically masked before the desired orders are coupled into the objective near the edge of the back aperture. The probe is derived from a photonic crystal fiber, which produces a broadband supercontinuum spanning 500 to 1200 nm. The continuum is passed through an interference filter (585 ± 5 nm), directed onto a computer-controlled delay stage, and coupled onto galvometer-mounted mirrors and a 4-f lens (200 mm) system to direct the beam to the objective. Pump and probe beams are coupled collinearly into the back aperture of a 100× apochromatic microscope objective (0.9 NA) with a dichroic beamsplitter. The focused probe spot is 340 nm fwhm at the sample position with a fluence of 0.9 mJ/cm^2. The sample is held on a piezoelectric X-Y stage at the focal point of the objective. The retroreflected probe is picked off with a 50/50 beamsplitter and directed onto one channel of a balanced photodetector. The delay-dependent change in probe reflectivity is measured with a digital lock-in amplifier (Stanford Research SR 844) phase locked to the pump modulation frequency (100 kHz). While acquisition time varies with the number of pixels in the image, the diffraction-limited pump−probe images shown in Figures 1 and 2 required approximately 1 min each to collect. SPPM images require acquisition times that are approximately 3 times longer, as multiple pump phases are required to reconstruct the image.

■ ASSOCIATED CONTENT

Supporting Information

The Supporting Information is available free of charge on the ACS Publications website at DOI: 10.1021/acsphotonics.6b00140.

Simulated line shapes for diffraction-limited and SPPM and conjugate space spectra of images in Figure 2 (PDF)

■ AUTHOR INFORMATION

Corresponding Author

*E-mail: erik.grumstrup@montana.edu.

Notes

The authors declare no competing financial interest.

■ ACKNOWLEDGMENTS

The authors would like to thank Prof. Jim Cahoon at the University of North Carolina Chapel Hill for providing nanowire samples. The authors gratefully acknowledge support from Montana State University and the Office of Basic Energy Sciences of the U.S. Department of Energy through Grant DE-SC0014128 for student (E.S.M., A.H.H.) support.

■ REFERENCES

(1) van Dijk, M. A.; Lippitz, M.; Orrit, M. Detection of Acoustic Oscillations of Single Gold Nanospheres by Time-Resolved Interferometry. *Phys. Rev. Lett.* **2005**, *95*, 267406.

(2) Staleva, H.; Hartland, G. V. Vibrational Dynamics of Silver Nanocubes and Nanowires Studied by Single-Particle Transient Absorption Spectroscopy. *Adv. Funct. Mater.* **2008**, *18*, 3809−3817.

(3) Mehl, B. P.; Kirschbrown, J. R.; House, R. L.; Papanikolas, J. M. The End Is Different than The Middle: Spatially Dependent Dynamics in ZnO Rods Observed by Femtosecond Pump−Probe Microscopy. *J. Phys. Chem. Lett.* **2011**, *2*, 1777−1781.

(4) Wang, R.; Ruzicka, B. A.; Kumar, N.; Bellus, M. Z.; Chiu, H.-Y.; Zhao, H. Ultrafast and spatially resolved studies of charge carriers in atomically thin molybdenum disulfide. *Phys. Rev. B: Condens. Matter Mater. Phys.* **2012**, *86*, 045406.

(5) Seo, M. A.; Yoo, J.; Dayeh, S. A.; Picraux, S. T.; Taylor, A. J.; Prasankumar, R. P. Mapping carrier diffusion in single silicon core-shell nanowires with ultrafast optical microscopy. *Nano Lett.* **2012**, *12*, 6334−8.

(6) Gabriel, M. M.; Grumstrup, E. M.; Kirschbrown, J. R.; Pinion, C. W.; Christesen, J. D.; Zigler, D. F.; Cating, E. E.; Cahoon, J. F.; Papanikolas, J. M. Imaging charge separation and carrier recombination in nanowire p-i-n junctions using ultrafast microscopy. *Nano Lett.* **2014**, *14*, 3079−87.

(7) Lo, S. S.; Shi, H. Y.; Huang, L.; Hartland, G. V. Imaging the extent of plasmon excitation in Au nanowires using pump-probe microscopy. *Opt. Lett.* **2013**, *38*, 1265−1267.

(8) Wong, C. T. O.; Lo, S. S.; Huang, L. Ultrafast Spatial Imaging of Charge Dynamics in Heterogeneous Polymer Blends. *J. Phys. Chem. Lett.* **2012**, *3*, 879−884.

(9) Grancini, G.; Maiuri, M.; Fazzi, D.; Petrozza, A.; Egelhaaf, H. J.; Brida, D.; Cerullo, G.; Lanzani, G. Hot exciton dissociation in polymer solar cells. *Nat. Mater.* **2012**, *12*, 29−33.

(10) Wong, C. Y.; Penwell, S. B.; Cotts, B. L.; Noriega, R.; Wu, H.; Ginsberg, N. S. Revealing Exciton Dynamics in a Small-Molecule Organic Semiconducting Film with Subdomain Transient Absorption Microscopy. *J. Phys. Chem. C* **2013**, *117*, 22111−22122.

(11) Wong, C. Y.; Cotts, B. L.; Wu, H.; Ginsberg, N. S. Exciton dynamics reveal aggregates with intermolecular order at hidden interfaces in solution-cast organic semiconducting films. *Nat. Commun.* **2015**, *6*, 5946.

(12) Hell, S. W.; Wichmann, J. Breaking the diffraction resolution limit by stimulated emission- stimulated-emission-depletion fluorescence microscopy. *Opt. Lett.* **1994**, *19*, 780−782.

(13) Wildanger, D.; Medda, R.; Kastrup, L.; Hell, S. W. A compact STED microscope providing 3D nanoscale resolution. *J. Microsc.* **2009**, *236*, 35−43.

(14) Heintzmann, R.; Cremer, C. Laterally Modulated Excitation Microscopy- Improvement of resolution by using a diffraction grating. *Proc. SPIE* **1998**, 185−196.

(15) Gustafsson, M. G. L.; Agard, D. A.; Sedat, J. W. Doubling the lateral resolution of wide-field fluorescence microscopy using structured illumination. *Proc. SPIE* **2000**, 141−150.

(16) Littleton, B.; Lai, K.; Longstaff, D.; Sarafis, V.; Munroe, P.; Heckenberg, N.; Rubinsztein-Dunlop, H. Coherent super-resolution microscopy via laterally structured illumination. *Micron* **2007**, *38*, 150−7.

(17) Rust, M. J.; Bates, M.; Zhuang, X. Sub-diffraction-limit imaging by stochastic optical reconstruction microscopy (STORM). *Nat. Methods* **2006**, *3*, 793−795.

DOI: 10.1021/acsphotonics.6b00140
ACS Photonics 2016, 3, 501−506

(18) Betzig, E.; Patterson, G. H.; Sougrat, R.; Lindwasser, O. W.; Olenych, S.; Bonifacino, J. S.; Davidson, M. W.; Lippincott-Schwartz, J.; Hess, H. F. Imaging Intracellular Fluorescent Proteins at Nanometer Resolution. *Science* **2006**, *313*, 1642−1645.
(19) Egerton, R. F. *Physical Principles of Electron Microscopy: An Introduction to TEM, SEM, and AEM*; Springer: New York, NY, 2005.
(20) Engel, A.; Müller, D. J. Observing single biomolecules at work with the atomic force microscope. *Nat. Struct. Biol.* **2000**, *7*, 715−718.
(21) Bechtel, H. A.; Muller, E. A.; Olmon, R. L.; Martin, M. C.; Raschke, M. B. Ultrabroadband infrared nanospectroscopic imaging. *Proc. Natl. Acad. Sci. U. S. A.* **2014**, *111*, 7191−6.
(22) Muller, E. A.; Pollard, B.; Raschke, M. B. Infrared Chemical Nano-Imaging: Accessing Structure, Coupling, and Dynamics on Molecular Length Scales. *J. Phys. Chem. Lett.* **2015**, *6*, 1275−84.
(23) Barnard, E. S.; Hoke, E. T.; Connor, S. T.; Groves, J. R.; Kuykendall, T.; Yan, Z.; Samulon, E. C.; Bourret-Courchesne, E. D.; Aloni, S.; Schuck, P. J.; Peters, C. H.; Hardin, B. E. Probing carrier lifetimes in photovoltaic materials using subsurface two-photon microscopy. *Sci. Rep.* **2013**, *3*, 2098.
(24) Wang, P.; Slipchenko, M. N.; Mitchell, J.; Yang, C.; Potma, E. O.; Xu, X.; Cheng, J. X. Far-field Imaging of Non-fluorescent Species with Sub-diffraction Resolution. *Nat. Photonics* **2013**, *7*, 449−453.
(25) Liu, N.; Kumbham, M.; Pita, I.; Guo, Y.; Bianchini, P.; Diaspro, A.; Tofail, S. A. M.; Peremans, A.; Silien, C. Far-Field Subdiffraction Imaging of Semiconductors Using Nonlinear Transient Absorption Differential Microscopy. *ACS Photonics* **2016**, DOI: 10.1021/acsphotonics.5b00716.
(26) Grumstrup, E. M.; Gabriel, M. M.; Cating, E. M.; Pinion, C. W.; Christesen, J. D.; Kirschbrown, J. R.; Vallorz, E. L.; Cahoon, J. F.; Papanikolas, J. M. Ultrafast Carrier Dynamics in Individual Silicon Nanowires: Characterization of Diameter-Dependent Carrier Lifetime and Surface Recombination with Pump−Probe Microscopy. *J. Phys. Chem. C* **2014**, *118*, 8634−8640.
(27) Grumstrup, E. M.; Cating, E. M.; Gabriel, M. M.; Pinion, C. W.; Christesen, J. D.; Kirschbrown, J. R.; Vallorz, E. L.; Cahoon, J. F.; Papanikolas, J. M. Ultrafast Carrier Dynamics of Silicon Nanowire Ensembles: The Impact of Geometrical Heterogeneity on Charge Carrier Lifetime. *J. Phys. Chem. C* **2014**, *118*, 8626−8633.
(28) Mukamel, S. *Principles of Nonlinear Optical Spectroscopy*; Oxford University Press: New York, 1995.
(29) Chung, C.-Y.; Hsu, J.; Mukamel, S.; Potma, E. O. Controlling stimulated coherent spectroscopy and microscopy by a position-dependent phase. *Phys. Rev. A: At., Mol., Opt. Phys.* **2013**, *87*, 033833.
(30) Hajek, K. M.; Littleton, B.; Turk, D.; McIntyre, T. J.; Rubinsztein-Dunlop, H. A method for achieving super-resolved widefield CARS microscopy. *Opt. Express* **2010**, *18*, 19263−19272.
(31) Chowdhury, S.; Dhalla, A.-H.; Izatt, J. Structured oblique illumination microscopy for enhanced resolution imaging of non-fluorescent, coherently scattering samples. *Biomed. Opt. Express* **2012**, *3*, 1841−1854.
(32) Park, J. H.; Lee, S.-W.; Lee, E. S.; Lee, J. Y. A method for super-resolved CARS microscopy with structured illumination in two dimensions. *Opt. Express* **2014**, *22*, 9854−9870.

DOI: 10.1021/acsphotonics.6b00140
ACS Photonics 2016, 3, 501−506